Evidence of blocking effects on 3-keV Ne^{7+} ions guided through nanocapillaries in polycarbonate

N. Stolterfoht and R. Hellhammer
Helmholtz-Zentrum Berlin für Materialien und Energie, D-14109 Berlin, Germany

B. Sulik and Z. Juhász
Institute of Nuclear Research (ATOMKI), H-4001 Debrecen, Hungary

V. Bayer and C. Trautmann
GSI Helmholtz-Zentrum, Materialforschung, D-64291 Darmstadt, Germany

E. Bodewits and R. Hoekstra
KVI Atomic Physics, University of Groningen, NL-9747 AA Groningen, The Netherlands

(Received 10 February 2011; published 10 June 2011)

We studied the dynamic properties of ion guiding through nanocapillaries etched in insulating polycarbonate (PC). Capillaries with diameters of 95 and 165 nm and a length of 10 μm were used. In a further sample, the capillaries had a diameter of 175 nm and a length of 30 μm. A few additional measurements were made using capillaries in polyethylene terephthalate (PET). The temporal evolution of the intensity and the angular distribution of the transmitted ions were studied by measuring transmission profiles as a function of the charge deposited on the sample surface. The tilt angle of the capillary axis was varied from 0° to 5°. The mean emission angle of the transmission profiles exhibit pronounced oscillations, similarly as in previous measurements using PET. However, for PC, nearly an order of magnitude more charge needs to be inserted into the capillaries to accomplish the oscillations. In contrast to PET, with PC, we observed a strong decrease of the profile intensities with irradiation time. This observation provides evidence of blocking effects on the ions, which are likely to be due to a repulsive field produced by significant charge deposition inside the PC capillaries.

DOI: 10.1103/PhysRevA.83.062901 PACS number(s): 61.85.+p, 34.50.Fa

I. INTRODUCTION

The transmission of ions through nanocapillaries has received considerable attention in the past few years. Pioneering work has been conducted with capillaries in metals wherein the ions undergo charge transfer processes producing hollow atoms that can be studied in free space [1,2]. When using capillaries in highly insulating materials, like polymers, charge patches are created inside the capillary wall. Sufficient charge buildup produces a repulsive electric field, which results in the deflection of the following ions. This deflection occurs at relatively large distances so that electron capture into the projectile is inhibited. Thus, the ions may be guided along the capillary axis maintaining their incident charge state during their passage even when the capillary axis is tilted with respect to the incident beam direction.

The initial exploration of the ion guiding phenomenon in insulating materials has made use of capillaries in polyethylene terephthalate (PET) polymers [3,4] (and references therein). Thereafter, several laboratories performed experimental studies of capillary guiding with PET [5–10], polycarbonate (PC) [7,11], SiO_2 [12], and Al_2O_3 [13–16]. Moreover, electrons were used as projectiles guided through capillaries in Al_2O_3 [17] and PET [18]. Also, single-glass capillaries [19–22] have been applied with the intention to produce submicrometer sized beams. Moreover, theoretical studies based on simulations and *ab initio* calculations have provided detailed insights into guiding mechanisms [23–26].

The essential part of the ion guiding is the self-organizing process, which governs the charge deposition inside the capillaries [3]. As shown in Fig. 1, the incident ions produce a dominant charge patch in the entrance region which, in turn, produces electric field components perpendicular to the capillary axes. With increasing deposition by the ions, the charge patch increases until the electrostatic field is just large enough to deflect the ions. Then, the ion deposition decreases and the charge patch reaches an equilibrium where the deposited current is equal to the current flowing away via the material conductivity. In this case, a significant number of ions is deflected in the direction of the capillary exit. The amount of charge in the entrance patch is rather independent of the incident ion current [27], which provides clear evidence that the material conductivity is governed by a nonlinear (exponential) conductivity law.

Apart from the dominant charge patch near the entrance region, additional weaker patches are temporarily produced further inside the capillaries [23]. Recent experimental studies about the temporary charge patches have been conducted [28–31], wherein oscillatory movements of the ion emission have been observed. The temporary patches play a significant role in the guiding process during the pre-equilibrium period represented by Fig. 1(a). They change their position and strength so that dynamic properties of the ion guiding become important. At equilibrium represented by Fig. 1(b), the secondary patches loose importance and the transmission stabilizes. Only a smaller charge patch may remain within the inner part to steer the ions primarily along the capillary axis. Small statistical fluctuations of this charge patch may widen the profile of the transmitted ions. Also, at the capillary exit, a radially symmetric field including perpendicular components is produced by charges deposited near the entrance region [23].

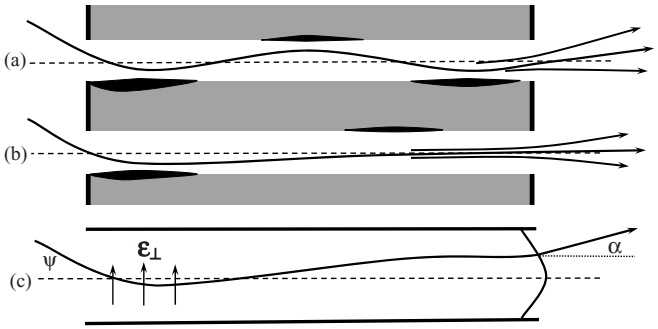

FIG. 1. Scenarios of ion guiding through capillaries in an insulating material. In (a) and (b), typical trajectories occurring in, respectively, the dynamic and the equilibrium period of the charge evolution are shown, where the black areas indicate charge patches [30]. In (c), the relevant quantities for the equilibrium are shown. The tilt angle is ψ. In the entrance region, the ions are deflected by perpendicular field components $\epsilon_{\perp}$. In the exit region, a contour line of a symmetric potential is given, causing the deflection by the angle α [23].

Thus, in the exit region, the ions are defocused, leading to a widening of the transmission profile as shown in Fig. 1(c).

To date, agreement exists about the general scope of the guiding mechanism; however, many details of the guiding properties are only partially understood. In particular, at various laboratories [5,7,11–14,16,32,33], different results were obtained for the ability of the capillaries to guide ions, referred to as guiding power. Evidently, the guiding power depends on properties and surface treatments of the samples. In view of the previous works, it is desirable to study the influence of the material properties on the ion guiding. In a recent work [7], the guiding power for PET and PC polymers were found to be consistent. However, for PC, the experiments have been performed with relatively high projectile energies. More information is needed about the dynamics of the ion guiding through capillaries in PC and PET for comparable energies.

In the present work, we investigate dynamic properties of 3-keV Ne^{7+} ions guided through PC capillaries in comparison with previous PET results. Similarly as for PET, the ions transmitted through PC capillaries show damped oscillations of the mean emission angle with increasing deposited charge. On the other hand, significant differences are observed in the oscillatory structures for the two polymers. For PC, nearly an order of magnitude more charge needs to be inserted into the capillaries to accomplish the oscillations. Furthermore, with PC, a strong intensity decrease of the transmitted ions is observed with increasing charge insertion. This intensity decrease, referred to as the blocking effect for the incident ions, may be attributed to a larger collection of charges inside the PC.

II. EXPERIMENTAL METHOD

The experiments were performed in an ultrahigh vacuum chamber mounted at the 14-GHz Electron Cyclotron Resonance (ECR) ion source of the ZERNIKE-LEIF facility at the KVI Groningen (Netherlands) [34]. The experimental method has been described before [30] so that only a few details are pointed out here. The vacuum chamber was used in a high-vacuum mode, i.e., the base pressure was some 10^{-8} mbar. The apparatus was set on high voltage to allow for the deceleration of the incident Ne^{7+} ions from 49 down to 3 keV. The ion current was varied within the range of 10–1000 pA. The beam was collimated to a diameter of ~1 mm with a divergence better than 0.2° full width at half maximum (FWHM).

TABLE I. Specific properties of the capillary samples used in this work. Given are the diameter d, the length L, and the density ρ of the capillaries.

Sample No.	Material	d (nm)	L (μm)	ρ (cm^{-2})
1	PC	165 ± 15	10	1×10^8
2	PC	95 ± 10	10	5×10^8
3	PC	175 ± 20	30	1×10^8
4	PET	100 ± 10	12	6×10^6

Cylindrical capillaries in PC polymers were prepared in the Department of Materialforschung at the GSI Helmholtz-Zentrum. They were produced by etching the tracks of 2-GeV gold ions in the PC polymer [35]. In Fig. 2, we show images obtained with scanning electron microscopy (SEM) to exhibit the density and diameters of the capillaries. The properties of the capillary samples are given in Table I. In Fig. 2(a), the foil sample of 10-μm thickness contains capillaries with a density of 10^8 cm^{-2} and a diameter of 165 nm. In Fig. 2(b), the sample of 10 μm thickness contains capillaries with a density of 5×10^8 cm^{-2} and a diameter of 95 nm. In Fig. 2(c), the sample of 30 μm thickness contains capillaries with a density of 10^8 cm^{-2} and a diameter of 175 nm The preparation of the capillaries in the PET foil has been described before in [7,33], where also images of the PET samples are shown. The PET capillaries with a density of 4×10^6 cm^{-2}, a length of 12 μm, and a diameter of 100 nm were obtained by etching tracks of 250-MeV krypton ions. To avoid a macroscopic chargeup of the sample surfaces, gold layers were deposited under 30° on the front and the back sides of the foils, forming film thicknesses of 10 for PC and 20 nm for PET.

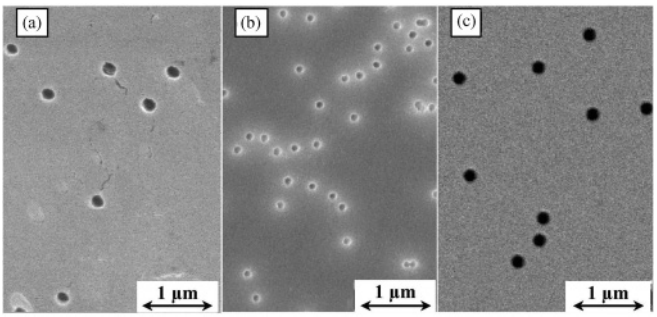

FIG. 2. SEM images of sample surfaces showing the capillary diameters and density used in the present experiments. In (a) and (b), the capillary diameters are 165 and 95 nm, respectively, and in (c), the diameter is 175 nm. The length of 1 μm is given in each panel to provide the scale of the horizontal and vertical dimensions.

The capillary foils were mounted at a goniometer, which allowed for a rotation of the capillary sample by the angles ψ and φ defined relative to the incident beam direction [3]. The rotation axes of the ψ and φ angles are both located within the capillary sample. The rotation axis of the ψ angle is vertical and coincides with the rotation axis of the spectrometer, whereas the rotation axis of the φ angle is horizontal. The tilt angle ψ is an important parameter in the present study, whereas the φ angle was kept constant after its zero value was fixed using an alignment laser. The PC and PET target foils were spanned into circular frames with an inner diameter of 7 mm. By moving the frame with the goniometer, the incident Ne^{7+} ion beam could be positioned at different spots within the target area. With the beam diameter of 1-mm FWHM, the ion beam could be located at five well-separated spots. Hence, the results described below for each tilt angle and diameter were obtained with fresh capillaries.

For the present experiments, it was important to use capillaries which are highly parallel. The angular spread of the capillary inclination was determined to be $\lesssim 0.2^\circ$ FWHM by measuring the transmission of high energy ions as a function of the tilt angle, for which the ion guiding effect is minor. This inclination is significantly smaller than the aspect angles of the capillaries. The small angular spread is a decisive condition for studying the time evolution of angular transmission profiles. When the capillaries are not parallel, the ions are first transmitted at angles smaller than the capillary tilt angle, since the ion transmission through nonparallel capillaries is favored before the ion guiding sets in. This spurious effect has clearly been observed with nonparallel capillaries of 2°-FWHM spread, for which ions were first detected at 0°, although the capillary sample was tilted by 5° [36]. After the ion guiding has started, the transmission profiles were shifted from 0° to their final value of 5°. Hence, for nonparallel capillaries, the spurious angular shift can be so large that it is difficult to observe the dynamics of the ion guiding through capillaries.

The neon ions emerging from the capillaries were analyzed with respect to their charge state, energy, and emission angle using an electrostatic 180° spectrometer, which could be rotated by the angle θ in the same plane as the tilt angle ψ. In the experiments, the angular distribution of the transmitted Ne^{7+} ions was measured for a fixed energy, which was equal to the incident one. The angular resolution of the analyzer was 0.2° FWHM. For the direct incident beam (without the capillary target), a Gaussian-like angular profile with a FWHM of 0.5° was acquired. This width is a composition of the beam width, its divergence, and the angular resolution of the analyzer. The energy resolution of the analyzer was 0.5%, which was sufficient to separate the charge states of the transmitted ions.

III. EXPERIMENTAL RESULTS

A. Transmission profiles

In the following, we study transmission profiles of 3-keV Ne^{7+} ions, whose incident charge state was preserved during the passage through the capillary. A transmission profile represents an angular distribution $dY(\theta,\phi = 0^\circ)/d\Omega$ of Ne^{7+} ions transmitted through the capillaries as a function of the observation (or emission) angle θ. The solid angle is given as $d\Omega = d\phi$. The angles θ and ϕ are defined relative to the incident beam direction. We recall that ϕ was fixed at 0° in the experiments.

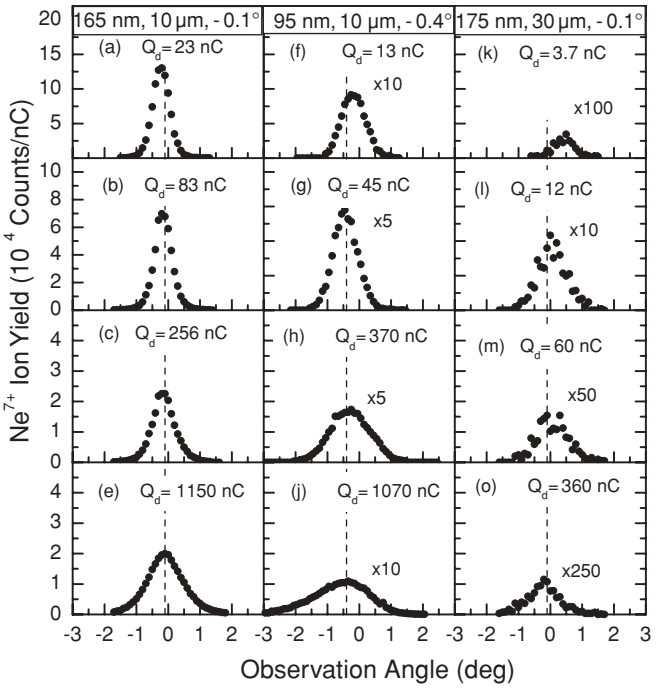

FIG. 3. Transmission profiles for 3-keV Ne^{7+} ions passing through capillaries in PC. The value for Q_d denotes the charge deposited at the foil surface prior to the profile acquisition. The tilt angles of the samples are $|\psi| \leqslant 0.4^\circ$. The left- and right-hand columns refer to capillaries with diameters of 165 and 175 nm, respectively, and with lengths of 10 and 30 μm. The middle column refers to capillaries of a diameter of 95 nm and a length of 10 μm.

Figures 3 and 4 show a series of selected transmission profiles for the tilt angles of $\psi \approx 0^\circ$ and $\psi = 5^\circ$, respectively. Similar results were obtained for 2° and 3°. The left-hand column entries show profiles obtained with capillaries of 165 nm in diameter and 10 μm in length. The middle column entries contain results for capillaries of 95 nm in diameter and 10 μm in length. The right-hand column entries contain data for capillaries of 175 nm in diameter and 30 nm in length. Each transmission profile is normalized to an integrated current of $Q_d = 1$ nC, which is the beam charge deposited on the front surface of the target foil. For a given incident beam current, the deposited charge is a measure of time. Each graph indicates the total charge Q_d collected till the instant when the profile is measured.

Figure 3 shows the temporal evolution of the transmission profiles for tilt angles close to 0°. It is recalled that the experimental uncertainty of setting the capillary at a given tilt angle is about ±0.2°. The exact tilt angle can only be determined after the experiment. The peak position of the transmission profiles is rather constant, i.e., there are only small deviations from the center value represented by a dashed line. However, the transmission profiles exhibit significant intensity losses with increasing charge deposition. The decrease of the ion intensity is particularly strong for the

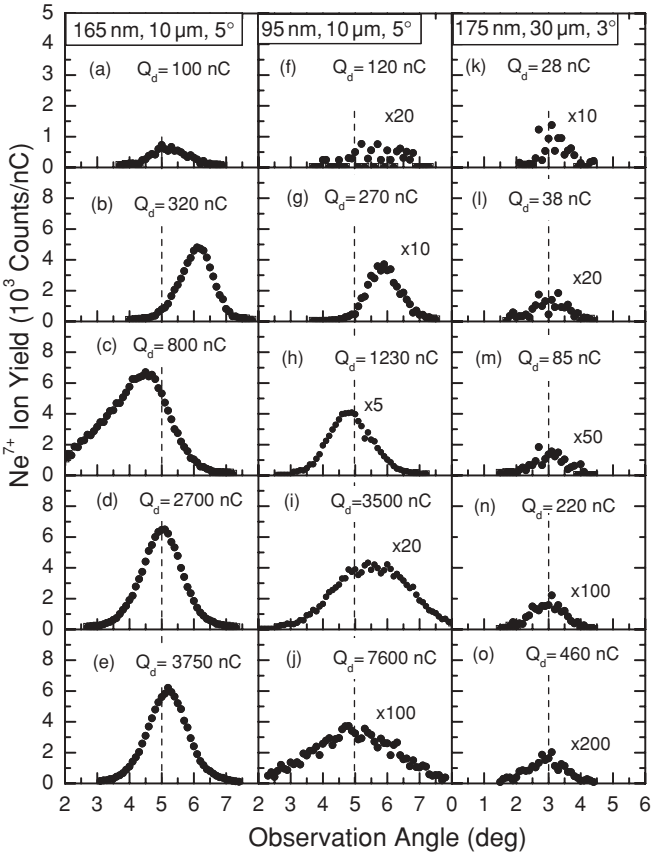

FIG. 4. Transmission profiles for 3-keV Ne^{7+} ions passing through capillaries etching in PC. The tilt angles of the capillaries are 5° and 3°. Further caption text as in Fig. 3.

foil of 30-μm thickness (right-hand column). This observation will be attributed to blocking effects on the ions traveling through the capillaries. We expect that the blocking effect is produced by charge deposition within the capillaries, since it is reduced at least by a factor of 2 after the sample has not been irradiated during the night.

In Fig. 4, transmission profiles are depicted for the tilt angles of 5° and 3°. In this case, the profile intensities first increase with deposited charge Q_d until a maximum is reached. Such an increase is expected since the ion guiding is primarily caused by the first charge patch, which needs some time to be formed. After the profiles have reached a maximum, their intensity decreases similarly as for the 0° tilt angle. Hence, the ion blocking occurs also for angles different from 0°.

For the foil thickness of 10 μm, the maximum position of the transmission profile exhibits oscillatory deviations from the center value of 5°, which is equal to the tilt angle. The maximum deviation from the center value is more than 1° [e.g., see Fig. 4(b)], which is larger than the aspect angle of 0.85° for the 165-nm capillaries. This observation provides evidence for the formation of secondary charge patches, which will be discussed in the next section. In contrast to the 10-μm capillaries, the transmission profiles for capillaries of 30 μm in length are rather constant in position (Fig. 4).

From the analysis of the transmission profiles, the FWHM σ_θ can be determined. For the tilt angle of 0°, the profile widths are first increasing with increasing charge deposition. Then,

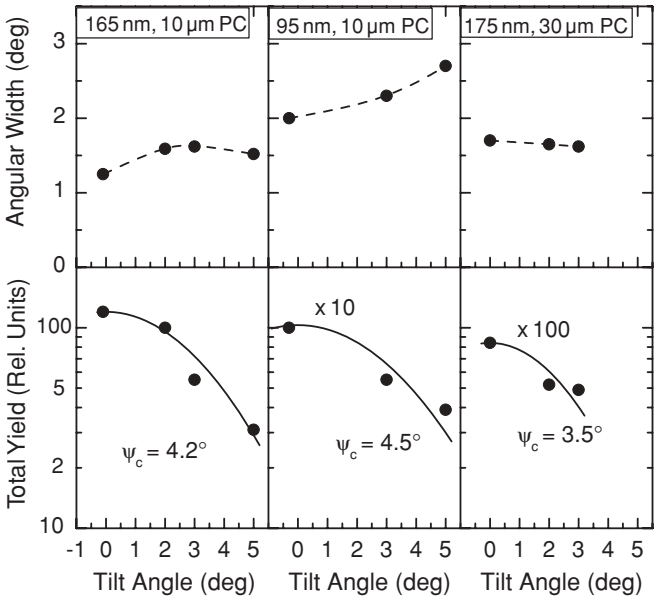

FIG. 5. Characteristic values of the transmission profiles given in Figs. 3 and 4. The diameter and length of the capillaries are given in each graph. In the upper row, the FWHM σ_θ is depicted and in the lower row the total yield $Y(\psi)$ is given as a function of the tilt angle ψ. The solid lines present fits with Gaussian functions. The guiding angle ψ_c is given in each panel (see text).

for larger charge deposition, the widths approach stable values which are shown in the upper row of Fig. 5. The stabilized values for 5° are also given in Fig. 5 together with additional results for 2° and 3°. We note that the 95-nm capillaries show a larger width than the 165-nm capillaries. This observation, which appears counterintuitive, is in accordance with a recent systematic study concerning the diameter dependence of various profile properties [9].

Next, we shall consider the total yield of the transmitted ions obtained by integration:

$$Y(\psi) = \int \frac{dY}{d\Omega}\, d\Omega. \tag{1}$$

Since in this work, only the ion yield with respect to the angle θ was measured, the integration over the angle ϕ was performed assuming that its dependence is described by a Gaussian function. The width σ_ϕ of the Gaussian was set to be equal to the width σ_θ of the transmission profile obtained for sufficiently large charge deposition [7].

As noted, the capability of insulating capillaries to guide ions at equilibrium is referred to as the guiding power.The fraction $f(\psi)$ of transmitted ions at equilibrium generally decreases with tilt angle ψ. The guiding power can be characterized by the *guiding angle* ψ_c for which the normalized transmission fraction drops as $f(\psi_c)/f(0) = 1/e$ [27]. To date, the guiding angle is accepted as a convenient parameter to quantify the guiding power. However, the definition of the guiding power has been introduced for the cases where the intensity of the transmitted ions reaches a constant equilibrium value with increasing charge deposition. Since for PC, we observe a final decrease of the profile intensity, the definition of the guiding angle ψ_c is somewhat ambiguous. Here, for each tilt angle we have taken the maximum value of the profile

intensity (see also the section below devoted to the blocking effect).

In the lower row of Fig. 5, the results of the maximum total yield are depicted as a function of the tilt angle ψ. The data are fitted with a Gaussian function

$$Y(\psi) = Y_{\max} \exp\left(-\frac{\sin^2\psi}{\sin^2\psi_c}\right), \tag{2}$$

which contains the guiding angle ψ_c as a fit parameter given in each panel in the lower row of Fig. 5. However, we recall that the derivation of the guiding angle involves uncertainties due to the decrease of the transmitted ion yield with extended charge deposition. This should be kept in mind when the present results for the guiding angle are compared with data obtained previously.

B. Oscillation of the profile position

As can be observed from Fig. 4, the transmission profiles change position when the charge deposition increases. Accordingly, the mean value of the ion emission angle varies. This mean angle was obtained by numerical integration using the well-known expression

$$\bar{\theta} = \frac{\int \theta\,(dY/d\Omega)d\theta}{\int (dY/d\Omega)d\theta}, \tag{3}$$

where $\phi = 0^\circ$ as mentioned before.

In Fig. 6, the mean emission angle of the transmitted ions is shown for the capillaries of 165 nm in diameter and 10 μm in length. The mean angle exhibits oscillatory variations, which are found to be similar for different tilt angles of $\psi = 2^\circ$, 3°, and 5°. To guide the eye, the corresponding crossing points (nodes) of the mean emission angle with the horizontal central line are connected by dashed-dotted curves. It is seen that corresponding nodes shift to higher values of the deposited charge as the tilt angle increases. The amplitude of the mean angle oscillation increases with increasing tilt angle.

For the tilt angle of 5°, the oscillatory displacements occur within the rather large angular range 4.1°–6.3°. Within this range, the mean angle appears to oscillate within three extremes (minima and maxima). The last extreme is not fully visible, since for the 5° tilt angle not enough data are available for larger charge deposition (Fig. 6). For the tilt angles of 2° and 3°, all three extremes can be seen. The oscillations of the mean emission angle with increased charge deposition are damped, and the angle approaches a constant value equal to the corresponding tilt angle (dashed line).

The oscillations of the profile position and their interpretation by the formation of charge patches within the capillaries have been extensively discussed before [28–31] so that only a few details are given here. Each extreme deviation of the mean emission angle corresponds to a charge patch so that in the present cases three charge patches are likely being produced. The most prominent charge patch, formed in the entrance region of the capillaries, is stable for larger charge deposition (steady state) whereas the other charge patches are only temporarily produced deeper within the capillary. In the steady state, a residual smaller patch is expected to remain within the downstream region, which has the effect to steer the ion beam essentially along the capillary axis [30].

In Fig. 7, the evolution of the mean angle is shown for the capillaries of 95 nm in diameter and 10 μm in length. The qualitative behavior of the data is similar as in the case of the 165-nm capillaries. The oscillatory structures are stretched to larger charge deposition values, and the their amplitudes increase with increasing tilt angle. Moreover, the oscillations

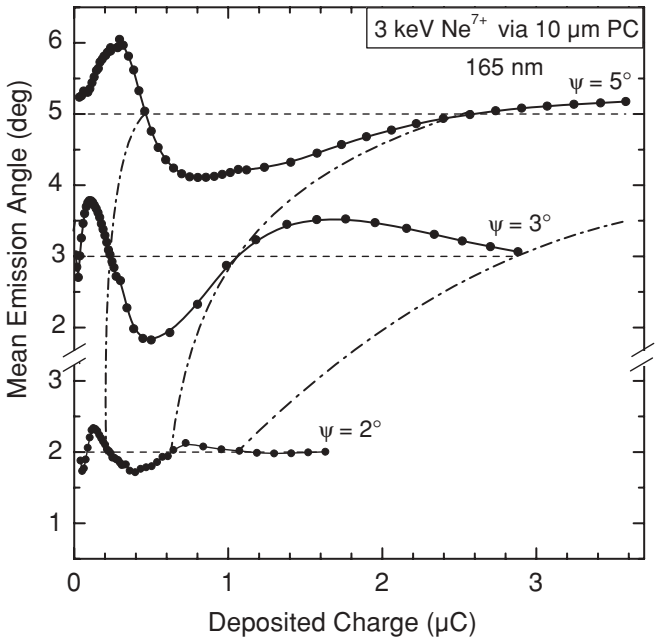

FIG. 6. Mean emission angle of the transmitted 3-keV Ne^{7+} ions for tilt angles of 2°, 3°, and 5°. The capillary diameter is 165 nm and its length is 10 μm. The dashed-dotted lines are drawn to guide the eye along the nodes of the mean angles. The horizontal dashed lines represent the central angle equal to the tilt angle.

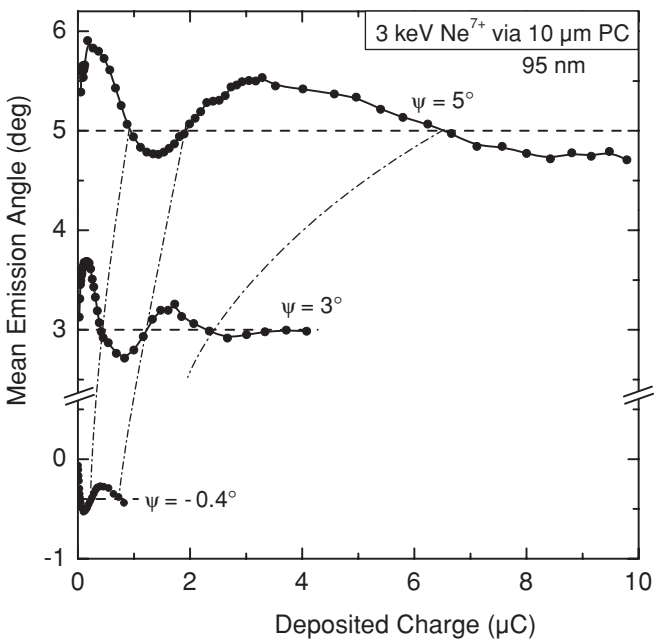

FIG. 7. Same as in Fig. 6, but for 95 nm capillaries and tilt angles of -0.4°, 3°, and 5°.

with increasing charge deposition are damped. (Note that the curve for the negative tilt angle of -0.4° shows the tiny oscillations, which are mirrored with respect to the positive tilt angles.) Altogether, the mean emission angle exhibits four extremes. For the tilt angle of 5°, the last extreme is only partially visible. Hence, we conclude that the present 95 nm capillaries involve four charge patches, which is one more than observed for the 165 nm capillaries.

Usually, the charge deposited on the foil surface is a convenient parameter to scale the capillary properties. However, it should be realized that for a given deposited charge Q_d, the charge $Q_{\rm in}$ that is inserted into an individual capillary depends on the capillary diameter. The inserted charge is obtained from [9]

$$Q_{\rm in} = Q_d \frac{a}{A} = Q_d \left(\frac{d}{D}\right)^2, \tag{4}$$

where a is the area of the capillary opening, and A is the area of the beam spot on the target sample. For example, with the beam base width of $D \approx 1.5$ mm and a capillary diameter of $d = 165$ nm, it follows that $a/A \simeq 12 \times 10^{-9}$. Hence, for the charge deposition of 1 μC, the inserted charge is about 10 fC per capillary. For the diameter of 95 nm, this conversion factor is a factor of 3 smaller.

To compare the mean emission angle for capillaries of different diameters, it is useful to plot the data as a function of the charge inserted into each capillary. In Fig. 8, this is done for the tilt angle of 5°. It is seen that the curve for the 95 nm oscillates faster than that for the 165 nm capillaries. Evidently, for the diameter of 95 nm, less charge is needed to form the patches responsible for the oscillatory behavior. A similar conclusion has previously been drawn from the comparison of 200- and 400-nm capillaries in PET [30]. From that work, the results for the 200-nm capillaries in 12-μm PET are depicted in Fig. 8(a). Qualitatively, the oscillations for the capillaries in PET are similar to those for PC. However, the oscillations for the capillaries in PET occur for much smaller inserted charges. We shall come back to this remarkable observation in the discussion section.

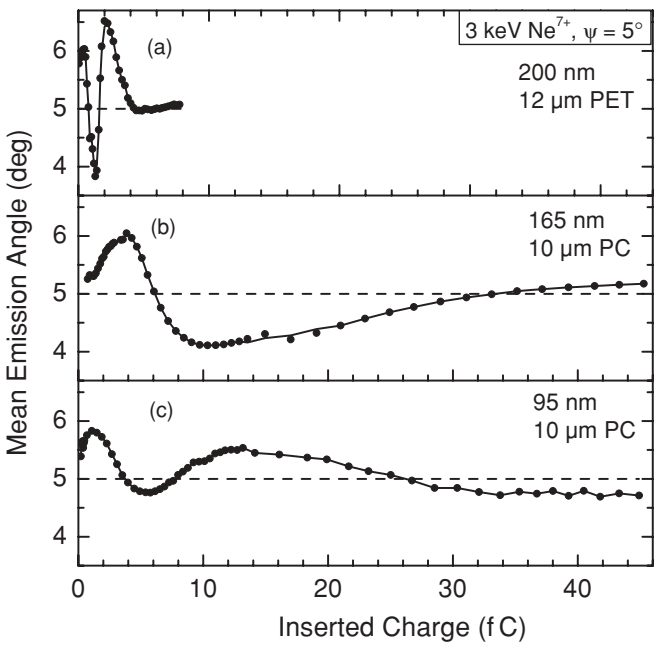

FIG. 8. Comparison of the mean emission angle for different type of capillaries as a function of the inserted charge $Q_{\rm in}$. The energy of the transmitted Ne^{7+} ions is 3 keV and the capillary tilt angle is 5°. The PET results in (a) for 200-nm capillaries are taken from Ref. [30].

C. Blocking of the transmission

In the following, we investigate the time evolution of the total yield Y of transmitted Ne^{7+} ions. First, the results for the PC samples are given for different tilt angle as a function of the deposited charge. Then, data for PC and PET are compared as a function of the charge inserted into the capillaries to point out significant differences between the two types of polymers.

Figure 9 shows the total ion yield for the capillaries in PC with a diameter of 165 nm and a length of 10 μm. The yields for the different tilt angles of -0.1°, 3°, and 5° show a similar behavior. However, the minima and maxima of the yield curves are shifted to higher deposited charges as the tilt angle increases. Moreover, in the case for 3° and 5°, the yields first increase from 0 to a maximum value before they start to drop. Unfortunately, not enough data are available for larger charge deposition to be able to conclude whether the yield approaches a constant value or finally drops to 0. The initial rising of the ion yield for nonzero tilt angles is a well-known feature which is associated with the buildup of the main charge patch in the entrance region of the capillaries (see Fig. 1).

Figure 10 shows the total ion yield for the capillaries in PC with a diameter of 95 nm and a length of 10 μm. In

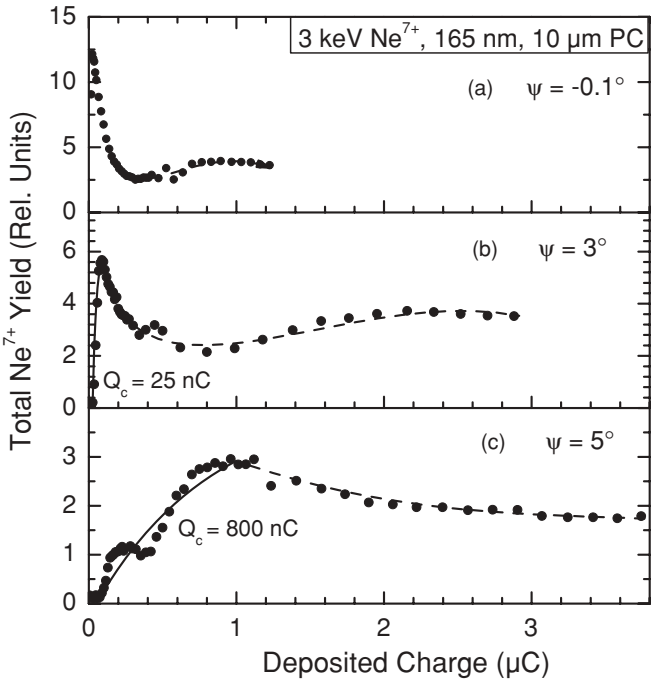

FIG. 9. Total ion yield Y of Ne^{7+} transmitted through capillaries in PC with a diameter of 165 nm and length of 10 μm plotted as a function of the deposited charge. In (a), (b), and (c) the tilt angles ψ are -0.1°, 3°, and 5°, respectively. The experimental data are fitted by Eq. (5), whose results are shown as solid lines together with the fit values of Q_c. The dashed lines are merely drawn to guide the eyes.

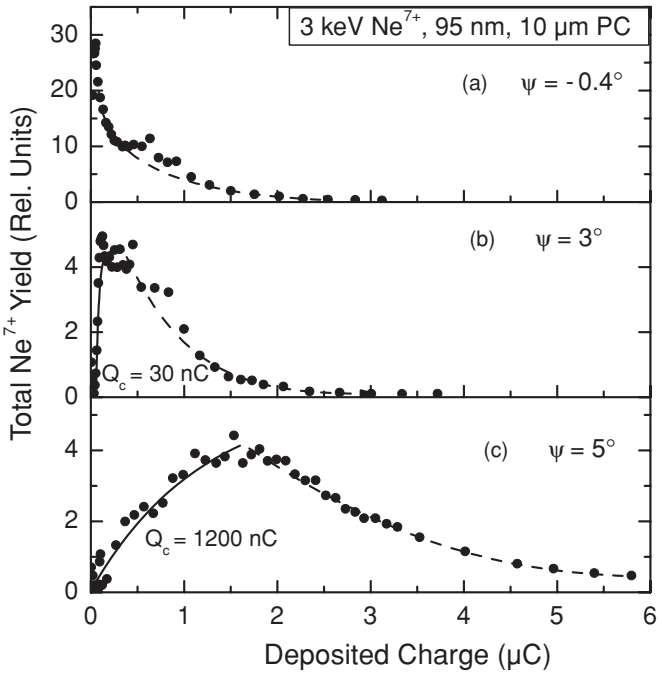

FIG. 10. Total ion yield Y of Ne^{7+} transmitted through capillaries in PC with a diameter of 95 nm and length of 10 μm plotted as a function of the deposited charge. In (a), (b), and (c) the tilt angles ψ are -0.4°, 3°, and 5°, respectively. The remainder of the legend as in the previous figure.

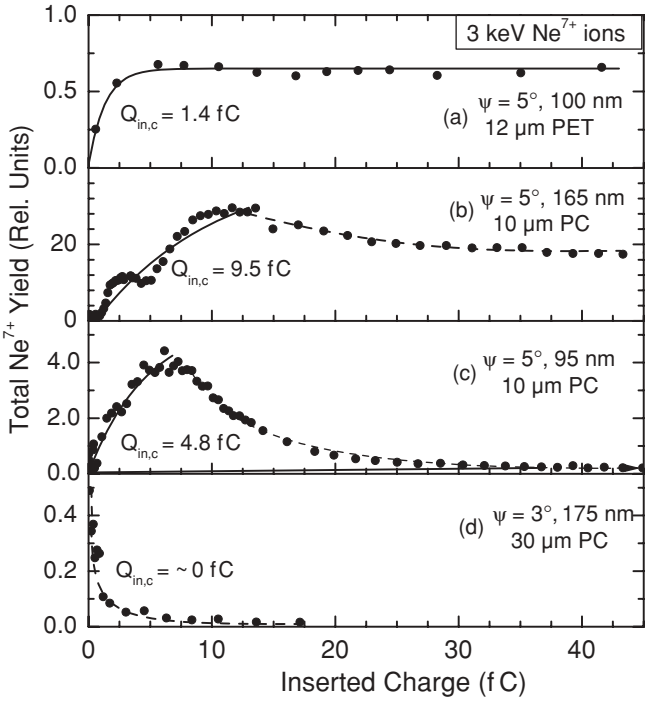

FIG. 11. Total ion yield Y of Ne^{7+} transmitted through capillaries in PET and PC plotted as a function of the inserted charge. The tilt angles ψ, the capillary diameter, and the length are indicated in each panel (a), (b), (c), and (d). The experimental data are fitted by Eq. (5). The results are shown as lines together with the fit values $Q_{\mathrm{in},c}$.

this case, the qualitative features are similar as those for the 165 nm capillary. However, all tilt angles have in common that the yield curves finally drop to 0. The structures observed in the curves for the tilt angles of -0.4° and 3° lie outside the statistical uncertainties. Such structures may also be present in the rising part for the tilt angle of 5° although they are difficult to localize due to limited statistics. Looking back at the rising part of the 5° data in Fig. 9(c), oscillatory deviations relative to the exponential fit curve can clearly be seen. The structures in the ion intensities should be considered in relation to the corresponding oscillations of the mean emission angle. More details about this relation are given in a recent work devoted to ion guiding in PET capillaries observing also neutralized projectiles [10].

The complete blocking for PC capillaries is a phenomenon, which has not been observed for ion guiding through capillaries in other types of materials. (We mention that a similar decrease has been found for electron transmission through capillaries in Al_2O_3 at 0° tilt angle [17].) A detailed blocking scenario, based on overcharged patches due to low surface conductivity, has been given in an simulation of ion guiding through PET capillaries [23]. For PET, previous measurements have shown a constant transmission after equilibrium is achieved [3,9,30]. However, the previous measurements have been performed in a limited charge deposition range. In the present work, we extended the experiment with 100 nm capillaries in 12-μm PET foils to charge deposition values, which exceeds those applied previously [9] by more than a factor of 5. The results for PET, shown in Fig. 11(a), are plotted as a function of the inserted charge. For PC, the ion transmission is found to be constant for rather high values of inserted charge, whereas within the same charge range, the ion yield is decreasing significantly for the capillaries in PC.

In Fig. 11(d), additional data are shown for the capillaries with the length of 30 μm and the diameter of 175 nm. The yield, obtained for the tilt angle of 3°, is strongly decreasing with the inserted charge. The same results were obtained for the tilt angles of 0° and 2°. For all tilt angles, the ion transmission shows a rapid drop of the ion yield, which indicates that significant blocking effects occur for the capillaries with the relatively large length of 30 μm.

Next, we approximate the initial increase of the ion yield for nonzero tilt angles with the exponential chargeup function [27]

$$Y(Q_d) = Y_0\left(1 - \exp\left[-\frac{Q_d - Q_s}{Q_c}\right]\right) \qquad (5)$$

for $Q_d > Q_s$, and $Y(Q_d) = 0$ otherwise. Here, we shall disregard the threshold value Q_s, since it is found to be minor for the cases studied. The characteristic charge Q_c was determined by fitting the total ion yield as shown in Fig. 11(a) for the PET capillaries. The fit results are given as a solid line in conjunction with the characteristic value of the inserted charge $Q_{\mathrm{in},c} = 1.4$ f C.

The analysis of the ion yields for PC capillaries by Eq. (5) is not so straightforward as it is for the PET capillaries. Due to the blocking effect, the ion yield is decreasing, which partially suppresses its initial rising. Hence, the rising curve is truncated in height and length, i.e., the equilibrium value, which is expected to be reached in the absence of the blocking effect, is not achieved. In particular, the blocking effect of the

ion transmission through the 30-μm capillaries is so strong that the rising part is not visible any more [see Fig. 11(d)]. Nevertheless, we have used the data for the 10-μm capillaries to fit the rising part by means of Eq. (5). In Figs. 9 and 10, the fit curves are shown for the tilt angles of 3° and 5° as solid lines together with the characteristic charge Q_c. However, we should keep in mind for the capillaries in PC that the fits by Eq. (5) involve uncertainties due to the truncation of the rising part caused by the blocking effect.

Figure 11 shows the fit values for the tilt angle of 5°, converted to the inserted charge $Q_{\mathrm{in},c}$, which allows for a comparison of the PC and PET capillaries. Comparing first the results for PC, we see that $Q_{\mathrm{in},c}$ is roughly proportional to the capillary diameter d, which is plausible as the charge in a bigger capillary is spread over a larger area. Furthermore, the $Q_{\mathrm{in},c}$ values for PC are relatively large in comparison with the result for PET. This observation is in accordance of the finding that significantly more charge is needed for PC to accomplish the angular oscillations discussed in the previous section.

IV. DISCUSSION AND CONCLUSIONS

The present study reveals several aspects concerning the guided transmission of highly charged ions through PC capillaries in comparison with the results for PET. We summarize the main features as follows:

(i) The analysis of the transmission profiles shows a relatively small width of ∼1.5° for the 165- and 175-nm capillaries, which increases to ∼2.5° for the 95-nm capillaries. The guiding angle is rather constant for varying diameter, and it fairly agrees with previous results for PET [7,30]

(ii) The temporal evolution of the transmission profiles exhibits pronounced oscillatory structures for PC capillaries with relatively small capillary diameters of 95 and 165 nm. For PET, such structures were observed only for capillary diameters equal to or larger than 200 nm [9,30].

(iii) As for PET, the oscillatory structures are stretched with increasing tilt angle. More extremes are found for the capillaries with smaller diameter, which is also in accordance with the PET results [30]. However, significantly more charge insertion is required for PC capillaries to accomplish the oscillations.

(iv) The total intensity for nonzero tilt angles shows the typical increase caused by the buildup of the entrance charge patch. As for PET, with increasing tilt angle, more charge is needed to maximize the intensity. However, in contrast to PET, the transmission through PC capillaries decreases after having reached a maximum value. This ion blocking is more significant for the diameter of 95 than for 165 nm, and drastic ion blocking is observed for capillaries with the length of 30 μm.

To interpret these results, we consider Fig. 12 showing a few characteristic ion trajectories incident with the tilt angle ψ. The z axis is chosen to be parallel to the capillary axis, and the x and y axis perpendicular to that. The incident ion deposition is responsible for the entrance patch shaded black. The charge patch produces the electric field $\epsilon(\mathbf{r})$ affecting the ions with the coordinates $\mathbf{r} = (x, y, z)$. Let us concentrate on

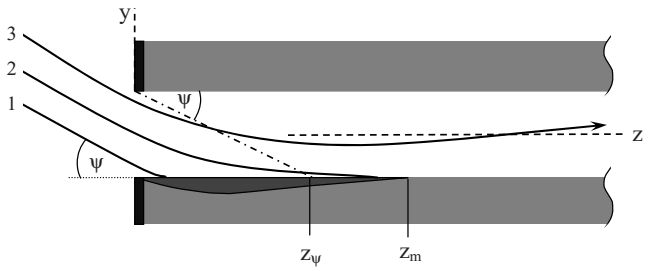

FIG. 12. Three typical trajectories of ions incident with the angle ψ on the entrance charge patch shaded black. The geometric and maximum lengths of the charge patch are indicated by z_ψ and z_m, respectively (see text).

central ion trajectories $\mathbf{r}(t)$ for which $x = 0$. The ion deflection angle by the repulsive field of the entrance patch is given by

$$\theta \approx \tan\theta = \frac{\Delta v_\perp}{v_\parallel}, \tag{6}$$

where $\Delta v_\perp$ is the velocity change in the perpendicular y direction, and $v_\parallel$ is the velocity parallel to the z direction [33]. For small deflection angles, $v_\parallel$ is set to be equal to the total velocity v.

The velocity $\Delta v_\perp$ change can be evaluated from the integration of the momenta received by the perpendicular field $\epsilon_\perp(\mathbf{r}(t))$, i.e., $\Delta v_\perp = M^{-1} q \int \epsilon_\perp(\mathbf{r}(t)) dt$, where M and q are the charge and the mass of the projectile, respectively. With $dt = dz/v$, we obtain the deflection angle as

$$\theta = \frac{q \int \epsilon_\perp(\mathbf{r}(z)) dz}{2E_p} = \frac{q\, U_e}{E_p}, \tag{7}$$

where E_p is the energy of the projectile, and U_e is a path integral of the perpendicular field along the trajectory of the incident ion

$$U_e = \frac{1}{2} \int \epsilon_\perp(\mathbf{r}(z)) dz. \tag{8}$$

We realize that Eq. (7) is redundant, since with the knowledge of the ion trajectory, the deflection angle is already given. However, this equation can be valuable when used with simplifying approximations of the ion trajectory or the electric field. Moreover, it is useful for understanding details of the guiding mechanisms.

For instance, let us look back at the guiding angle defined by Eq. (2). This guiding angle may be obtained as [33]

$$\psi_c = \frac{q\, U}{E_p}, \tag{9}$$

where the parameter U has been introduced as an effective potential experienced by the ions traversing the capillary entrance region (Fig. 1). Indeed, U has the dimension of a potential. However, comparison of Eqs. (9) and (7) shows that U can be identified as a path integral of the perpendicular field averaged over all ion trajectories. We note that a different interpretation of U has been given in Ref. [31].

Next, we consider the discharge of the entrance patch. Its charge produces a field $\epsilon_\parallel$ along the capillary wall, which predominantly causes a current flow in the direction of the

sample surface (which is covered by a grounded metallic film). However, the current may also flow in the opposite direction widening the charge patch [23]. For the discharge of the entrance patch, it can be assumed that the surface conductivity σ_s is more important than the bulk conductivity [37,38]. Using the Frenkel–Poole process for charge transport via tunneling from deep trap states [39], the surface current density can be expressed as

$$j = \epsilon_{\|}\sigma_s \exp\left(\sqrt{\frac{\epsilon_{\|}}{\epsilon_c}}\right). \tag{10}$$

This formula is a revised version of that given in Ref. [27], which has experimentally been confirmed. The parameter ϵ_c is a characteristic field governing the exponential increase of the surface current. The formula implies two regions where for $\epsilon_{\|} \ll \epsilon_c$, the current follows a linear dependence of the field (as in Ohm's law), and for $\epsilon_{\|} \gtrsim \epsilon_c$, the current is determined by a nonlinear (exponential) field dependence. The exponential increase of the current density implies that the charge collection and the field saturate. In fact, a further increase of the field would would lead to an electrical breakthrough. We note that this electrical break-through does not occur via the bulk of the polymer but along the capillary surfaces. For PET, the surface breakthrough value has experimentally been determined to be $\sim$100 V/μm [7].

The guiding scenario resulting from the Eqs. (7) and (10) reveals essential features. The ions, incident at the capillary bottom, enter into the capillary wall as indicated by the trajectory of type 1 (Fig. 12). When the charge deposition becomes sufficiently large, the perpendicular field $\epsilon_{\perp}$ saturates within a certain z range, which is roughly equal to the length z_{ψ} indicated in Fig. 12. Then, if the field is not sufficient for a full deflection to the exit, the range of charge deposition will be expanded, which is realized by ion trajectories of type 2. Finally, with the field of the extended charge patch, certain ions are deflected to the capillary exit as indicated by the trajectory of type 3. Hence, the self-organizing mechanism of ion guiding is not exclusively based on an increase of the charge but also on the extension of the entrance charge patch along the capillary axis. This becomes more evident, when Eq. (8) is rewritten as $U_e = z_m\widehat{\epsilon}_{\perp}/2$, where $\widehat{\epsilon}_{\perp} = \int \epsilon_{\perp}(\mathbf{r}(z))dz/z_m$ is the perpendicular field averaged over the length z_m of the charge patch (see Fig. 12).

For smaller tilt angles, it is evident that it requires less time of charge insertion into the capillaries to achieve the guiding conditions. The charge deposition length increases for decreasing tilt angle so that less charge is needed to achieve the ion deflection to the capillary exit. Therefore, the initial rise of the ion intensity, governed by the characteristic charge Q_c, occurs faster for smaller tilt angles, which is in agreement with the experimental observation mentioned in (iv). Moreover, the oscillation of the mean emission angle is faster for smaller tilt angles. The relation between Q_c and the oscillation frequency together with its damping has already been noted for PET [30]. It is plausible that with the approach of the total yield to its equilibrium value, the oscillation of the mean angle is damped so that it also approaches its final value.

The main new features of the PC capillaries are the relatively large charge insertion required to accomplish the oscillation and the blocking of the ion intensity. We expect that the two phenomena are related. For PC, it appears that the surface conductivity is rather small so that more charge stays within the capillaries. To roughly estimate the repulsive potential along the capillary axis, we used the quantity $Q_{\mathrm{in},c}$ (Fig. 11) as a measure for the equilibrium charge deposited within the entrance patch [27]. The length of entrance patch was assumed to be equal to z_{ψ} (Fig. 12) and the tilt angle was set equal to 5°. For both PC samples, we obtained a maximum potential of about 430 V at the center of the entrance patch, which is just sufficient to fully block 3-keV Ne^{7+} ions. On the other hand, for the PET sample, we obtained a corresponding potential of about 100 V, which is insufficient to suppress the ions. Also, it should be added that for 10-keV Ne^{7+} ions, no significant blocking in PC capillaries have been found [7]. It is evident that the blocking decreases with increasing ion energy.

Moreover, it is expected that the neighboring capillaries contribute to the creation of this center potential. Similar contributions have been evaluated for the potential at the capillary exit [23,25]. Note from Table I that the capillary density is significantly higher for PC than for PET. Also, the influence of the neighboring capillaries is consistent with the observation that the blocking effect is more significant for the 95-nm capillaries, which have a factor of 5 higher density than the 165-nm capillaries. Moreover, the scenario of the charge transport in the center part of the capillaries is consistent with the mention in (iv) that the blocking is more pronounced for a greater length. In this case, it is plausible that the inner wall of the capillaries collects more charge. Also, we recall that the blocking is more significant for smaller tilt angles, and it maximizes for 0°. For smaller tilt angles, more current is transported through the capillaries so that the charge collection is likely to increase.

The differences in the ion guiding by PC and PET capillaries are influenced by their material properties. The dielectric constant is close to 3 for both types of polymers. Also, the surface conductivities are similar in both cases, i.e., close to $\sim 10^{-16}$ S [37,38]. However, the material properties may be affected by impurities. Moreover, the surface conductivity depends strongly on the water absorption. The water absorption coefficient for PET is an order of magnitude larger than that for PC. For PET in air, it has been shown that the surface conductivity increases by four orders of magnitude when the relative humidity changes from 30 to 80% [38]. The higher water absorption for PET could explain the absence of the ion blocking, since charges are more readily removed from the inside of the capillaries.

The influence of the relative humidity demonstrates that the material properties may strongly depend on the conditions under which the capillaries were prepared. The present experimental observations suggest differences between the electrical surface properties of PC and PET. We were able to explain several details of the present results by means of model considerations. In particular, we provided some plausible reasons for the ion blocking observed for PC. Although a definite explanation is still missing, the study of neighboring capillaries appears to be a promising task. In this connection, emphasis should be given to reproducible conditions of the capillary production. We expect that future experimental and theoretical effort is needed to gain conclusive information about the dynamics of the ion guiding.

ACKNOWLEDGMENTS

We are indebted to Grigori Pokhil for several stimulating discussions. B.S. and Z.J. were supported by the Hungarian National Science Foundation OTKA (Grant No. K73703). This experiment was performed at the distributed LEIF-Infrastructure at ZERNIKE-LEIF. The work was financially supported by the European Network ITSLEIF under the Grant No. RII3-026015.

[1] S. Ninomiya, Y. Yamazaki, F. Koike, H. Masuda, T. Azuma, K. Komaki, K. Kuroki, and M. Sekiguchi, Phys. Rev. Lett. **78**, 4557 (1997).

[2] K. Tökési, L. Wirtz, C. Lemell, and J. Burgdörfer, Phys. Rev. A **61**, 020901 (2000).

[3] N. Stolterfoht, J. H. Bremer, V. Hoffmann, R. Hellhammer, D. Fink, A. Petrov, and B. Sulik, Phys. Rev. Lett. **88**, 133201 (2002).

[4] R. Hellhammer, P. Sobocinski, Z. D. Pešić, D. Fink, J. Bundesmann, B. Sulik, and N. Stolterfoht, Nucl. Instrum. Methods Phys. Res., Sect. B **233**, 213 (2005).

[5] G. Víkor, R. R. Kumar, Z. Pešić, N. Stolterfoht, and R. Schuch, Nucl. Instrum. Methods Phys. Res., Sect. B **233**, 218 (2005).

[6] Y. Kanai, M. Hoshino, T. Kambara, T. Ikeda, R. Hellhammer, N. Stolterfoht, and Y. Yamazaki, Nucl. Instrum. Methods Phys. Res., Sect. B **258**, 155 (2007).

[7] N. Stolterfoht, R. Hellhammer, Z. Juhász, B. Sulik, V. Bayer, C. Trautmann, E. Bodewits, A. J. de Nijs, H. M. Dang, and R. Hoekstra, Phys. Rev. A **79**, 042902 (2009).

[8] M. Kreller, G. Zschornak, and U. Kentsch, J. Phys.: Conf. Ser. **163**, 012090 (2009).

[9] N. Stolterfoht, R. Hellhammer, Z. Juhász, B. Sulik, E. Bodewits, H. M. Dang, and R. Hoekstra, Phys. Rev. A **82**, 052902 (2010).

[10] Z. Juhász, B. Sulik, R. Rácz, S. Biri, R. J. Bereczky, K. Tökési, Á. Köver, J. Pálinkás, and N. Stolterfoht, Phys. Rev. A **82**, 062903 (2010).

[11] D. Li, Y. Wang, Y. Zhao, G. Xiao, D. Zhao, Z. Xu, and F. Li, Nucl. Instrum. Methods Phys. Res., Sect. B **267**, 469 (2009).

[12] M. B. Sahana, P. Skog, G. Víkor, R. T. Rajendra Kumar, and R. Schuch, Phys. Rev. A **73**, 040901 (2006).

[13] S. Mátéfi-Tempfli *et al.*, Nanotechnology **17**, 3915 (2006).

[14] P. Skog, I. L. Soroka, A. Johansson, and R. Schuch, Nucl. Instrum. Methods Phys. Res., Sect. B **258**, 145 (2007).

[15] Y.-F. Chen *et al.*, Chin. Phys. B **18**, 2739 (2009).

[16] Z. Juhász *et al.*, Nucl. Instrum. Methods Phys. Res., Sect. B **267**, 321 (2009).

[17] A. R. Milosavljević, G. Víkor, Z. D. Pešić, P. Kolarž, D. Šević, B. P. Marinković, S. Mátéfi-Tempfli, M. Mátéfi-Tempfli, and L. Piraux, Phys. Rev. A **75**, 030901(R) (2007).

[18] S. Das, B. S. Dassanayake, M. Winkworth, J. L. Baran, N. Stolterfoht, and J. A. Tanis, Phys. Rev. A **76**, 042716 (2007).

[19] T. Ikeda, T. M. Kojima, Y. Iwai, Y. Kanai, T. Kambara, T. Nebiki, T. Narusawa, and Y. Yamazaki, J. Phys.: Conf. Ser. **58**, 68 (2007).

[20] A. Cassimi *et al.*, Nucl. Instrum. Methods Phys. Res., Sect. B **267**, 674 (2009).

[21] R. Bereczky, G. Kowarik, F. Aumayr, and K. Tökési, Nucl. Instrum. Methods Phys. Res., Sect. B **267**, 317 (2009).

[22] G. Kowarik, R. J. Bereczky, F. Aumayr, and K. Tökési, Nucl. Instrum. Methods Phys. Res., Sect. B **267**, 2277 (2009).

[23] K. Schiessl, W. Palfinger, K. Tökési, H. Nowotny, C. Lemell, and J. Burgdörfer, Phys. Rev. A **72**, 062902 (2005).

[24] K. Schiessl, W. Palfinger, K. Tökési, H. Nowotny, C. Lemell, and J. Burgdörfer, Nucl. Instrum. Methods Phys. Res., Sect. B **258**, 150 (2007).

[25] K. Schiessl, C. Lemell, K. Tökési, and J. Burgdörfer, J. Phys.: Conf. Ser. **163**, 012081 (2009).

[26] K. Schiessl, K. Tökési, B. Solleder, C. Lemell, and J. Burgdörfer, Phys. Rev. Lett. **102**, 163201 (2009).

[27] N. Stolterfoht, R. Hellhammer, J. Bundesmann, D. Fink, Y. Kanai, M. Hoshino, T. Kambara, T. Ikeda, and Y. Yamazaki, Phys. Rev. A **76**, 022712 (2007).

[28] P. Skog, H. Q. Zhang, and R. Schuch, Phys. Rev. Lett. **101**, 223202 (2008).

[29] Y. Kanai, M. Hoshino, T. Kambara, T. Ikeda, R. Hellhammer, N. Stolterfoht, and Y. Yamazaki, Phys. Rev. A **79**, 012711 (2009).

[30] N. Stolterfoht, R. Hellhammer, D. Fink, B. Sulik, Z. Juhász, E. Bodewits, H. M. Dang, and R. Hoekstra, Phys. Rev. A **79**, 022901 (2009).

[31] H. Q. Zhang, P. Skog, and R. Schuch, Phys. Rev. A **82**, 052901 (2010).

[32] M. Fürsatz, W. Meissl, S. Pleschko, I. C. Gebeshuber, N. Stolterfoht, H. P. Winter, and F. Aumayr, J. Phys.: Conf. Ser. **58**, 319 (2007).

[33] N. Stolterfoht, R. Hellhammer, J. Bundesmann, and D. Fink, Phys. Rev. A **77**, 032905 (2008).

[34] M. Unipan, A. Robin, D. F. A. Winters, R. Morgenstern, and R. Hoekstra, Phys. Rev. A **74**, 062901 (2006).

[35] G. Pépy, P. Boeseck, A. Kuklin, E. Manceau, B. Schiedt, Z. Siwy, M. Toulemonde, and C. Trautmann, J. Appl. Crystallogr. **40**, s388 (2007).

[36] N. Stolterfoht *et al.*, Nucl. Instrum. Methods Phys. Res., Sect. B **225**, 169 (2004).

[37] Datasheets for PC (Lexan) from Sabic Innovative Plastics™ [www.sabic-ip.com].

[38] Datasheets for PET (Mylar) from DuPont Teijin Films™ [www.dupontteijinfilms.com].

[39] Frenkel–Poole, Phys. Rev. **54**, 647 (1938).